Article

Not peer-reviewed version

Decomposition Rate and Microplastic Residue Formation of Photodegradable Resin-Coated Controlled-Release Fertilizers (CRFs)

Hyeong-Wook Jo , Joon-Seok Lee , Il Jang , Young-Il Cho , Joon-Kwan Moon *

Posted Date: 7 March 2026

doi: 10.20944/preprints202603.0569.v1

Keywords: controlled-release fertilizer; decomposition kinetics; microplastic; residue formation

 doi:10.20944/preprints202603.0569.v1

Article

Decomposition Rate and Microplastic Residue Formation of Photodegradable Resin-Coated Controlled-Release Fertilizers (CRFs)

Hyeong-Wook Jo [1], Joon-Seok Lee [2], Il Jang [2], Young-Il Cho [3] and Joon-Kwan Moon [4,*]

[1] Hansalim Agri-Food Analysis Center, Hankyong National University Industry Academic Cooperation Foundation, Suwon 16500, Republic of Korea

[2] FarmHannong Crop Protection Research Center, Nonsan 33010, Republic of Korea

[3] FarmHannong Co., Ltd, Seoul. 07320, Republic of Korea

[4] Department of Plant Resources and Landscape Architecture, Hankyong National University, Anseong 17579, Republic of Korea

* Correspondence: jkmoon@hknu.ac.kr; Tel.: +82-31-670-5083

Abstract

This study investigates the decomposition kinetics and microplastic residue formation of the polymer-coated controlled-release fertilizers (CRFs) LN40 and Eco-LN40 under simulated photodegradation conditions. Eco-LN40, containing TiO_2 as a photocatalyst, achieved complete decomposition (100 ± 2%) after 60 days of xenon-arc irradiation ($p < 0.05$), whereas LN40 achieved only 14%–31% decomposition. Analytical characterization using TED-GC/MS, FTIR, and Raman spectroscopy confirmed that polyethylene (PE) signals completely disappeared in Eco-LN40 but persisted in LN40, indicating that microplastics did not form and that there was total oxidation into CO_2 and H_2O. SEM–EDS revealed Ti enrichment and surface fragmentation consistent with photoinduced radical oxidation. This study provides qualitative and mechanistic evidence that TiO-catalyzed photodegradation can eliminate polymer residues, mitigate the risk of microplastic contamination in agricultural soils, and support carbon-neutral fertilizer technologies.

Keywords: controlled-release fertilizer; decomposition kinetics; microplastic; residue formation

1. Introduction

Compared with conventional fertilizers, controlled-release fertilizers (CRFs) enhance nutrient use efficiency and mitigate environmental losses [1–3]. CRFs incorporate polymeric coatings that regulate nutrient diffusion, thereby synchronizing nutrient availability with plant uptake and reducing nutrient leaching and volatilization [4]. Due to their agronomic advantages, CRFs are increasingly used worldwide to facilitate sustainable agriculture. However, the widespread use of polymer-coated fertilizers has raised concerns regarding the persistence and degradation of their coating materials [5]. Most CRF coatings are composed of synthetic polymers, such as polyethylene, polyurethane, or polyolefin derivatives, which are known for their high chemical stability and resistance to biodegradation [6]. When exposed to sunlight, temperature fluctuations, and moisture, polymer coating materials undergo photooxidative degradation and fragmentation, leading to the formation of microplastics [7]. Microplastics, defined as plastic fragments <5 mm in size, are persistent contaminants of global concern [8,9]. They can absorb organic pollutants and metals, alter soil structures, and interfere with microbial and plant functions [10]. Recent studies indicate that CRF coatings are a significant but overlooked source of microplastics in soils [11,12]. Thus, there is an urgent need to investigate the degradation of CRF coatings under environmental conditions.

Although photodegradation is considered a key pathway in polymer weathering, it rarely leads to the complete mineralization of carbon dioxide and water [13]. Incomplete oxidation may result in

 doi:10.20944/preprints202603.0569.v1

the formation of smaller polymeric fragments that persist as microplastics [14]. This indicates that the photodegradation of CRFs may transform fertilizer coatings into secondary pollutants, posing potential risks to soil health, crop safety, and aquatic ecosystems [5,12].

Despite these implications, research on CRFs has largely focused on nutrient release behavior and coating efficiency, whereas research into the environmental transformation of coating materials has been relatively neglected [4,6]. The empirical confirmation of microplastic formation during CRF degradation remains limited, and the mechanistic pathways linking photodegradation to microplastic generation have not been fully elucidated. The presence of microplastics in CRFs containing photocatalysts was examined to address these issues. Photocatalysts participate in photochemical reactions when exposed to light. When a photocatalyst containing TiO_2 is exposed to light, electrons and holes are effectively separated and react with oxygen in air or water to generate radical species such as O **. The holes (h^+) in TiO_2 react with water to produce hydroxyl radicals (OH*). These radicals attack the C–C and C–H bonds of the surrounding polyethylene (PE) chains, forming CO_2 or generating HO_2* radicals, which continue to attack and break PE chains. Through these continuous reactions, the plastic is gradually degraded into CO_2, H_2O, and intermediate compounds such as carboxyl and carbonyl groups. The mechanisms of TiO_2 polymer degradation under light exposure have been well established and documented by numerous researchers [15–18].

This study aimed to confirm that photocatalyst-containing CRFs do not produce microplastics during photodegradation using spectroscopy, microscopy, and analytical techniques.

2. Materials and Methods

2.1. Materials

For the photo-degradation experiment, the 'LN40' and 'Eco-LN40' polymer-coated controlled-release fertilizers (CRFs) sold by Farmhannong were used. 'LN40' does not contain a photocatalyst, whereas 'Eco-LN40' contains TiO_2. The coating materials consisted of low-density polyethylene (LDPE) and ethylene vinyl acetate (EVA) resins. Before use, all fertilizers were sieved to a particle size of 3–4 mm

2.2. Photo-Degradation Experiments

The CRFs were photodegraded under simulated sunlight using a xenon arc lamp chamber (wavelength range 300–800 nm, energy range 400 W/m^2), namely, a Suntest CPS+ (ATLAS, IL, USA). The samples were evenly spread on alumina Petri dishes to ensure uniform irradiation. The temperature inside the chamber was maintained at 55 ± 2 °C. The exposure durations were set to 0, 10, 20, 30, 40, 50, and 60 d to simulate progressive weathering. This experiment was conducted using a sun tester in accordance with the ASTM G151-19, ASTM G155-21, ASTM D 5071, and KS M 4892-1 standard test methods [19–22].

2.3. Decomposition Rate

The decomposition rate was calculated using the gravimetric method. However, because the coating shell contains both resin and mineral components, only the resin content within the coating layer was used for the calculation. The formulas used to calculate the resin contents of LN40 and Eco-LN40 are presented in Table 1.

Table 1. Decomposition rates (%) of LN40 and Eco-LN40.

	Formula
	(Initial weight – Measured weight) / (Initial weight × Resin content of LN40$^{(1)}$) × 100
	(Initial weight – Measured weight) / (Initial weight × Resin content of Eco-LN40$^{(2)}$) × 100

 doi:10.20944/preprints202603.0569.v1

(1) Resin content of LN40 = 0.48 (based on TGA analysis of the resin in the coating material) (2) Resin content of Eco-LN40 = 0.481 (based on TGA analysis of the resin in the coating material)

2.4. Characterization of Surface Morphology and Elemental Analysis

The surface morphologies of the CRF coatings before and after photodegradation were observed using scanning electron microscopy (SEM) and energy dispersive spectroscopy (EDS; JSM-7001F, JEOL, Tokyo, Japan). Before imaging, the samples were coated with a thin layer of gold under vacuum. Changes in surface roughness, cracking, and fragmentation were observed at 50,000 × magnification. The detailed specifications of the instrument are listed in Table 2.

Table 2. SEM/EDS conditions.

SEM-EDS	
Instrument	JSM-7001F (JEOL, Tokyo, Japan)
Magnification	10 (WD 40 mm) to 1,000,000×
Accelerating voltage	0.5–30 kV or wider
Probe current	1×10^{-12} to 2×10^{-7} A
Electron gun	Schottky type field emission gun

2.5. Thermal Extraction Desorption Gas Chromatograph Mass Spectrometer (TED-GC/MS)

TED-GC/MS analysis was performed to confirm the presence of PE [23]. GC-MS was performed using a 5977 B mass spectrometer and an 8890 gas chromatography system (Agilent, Santa Clara, CA, USA), and TED was performed using an MPS-TDU (Gerstel, Mülheim, Germany). The detailed specifications of the instruments are listed in Table 3.

Table 3. TED-GC/MS conditions.

Thermal Extraction Desorption	
Instrument	MPS-TDU (Gerstel, Mülheim, Germany)
Coupling temp.	240 °C
Desorption mode	Solvent vent
Desorption temp.	200 °C
CIS initial temp.	−100 °C
CIS end temp.	270 °C
Absorber	PDMS (Sorbstar)
Gas chromatography conditions	
Instrument	8890 (Agilent, Santa Clara, CA, USA)
Column	ZB-5MS UI (30 m × 0.25 mm, 0.25 µm, Phenomenex, Torrance, CA, USA)
Flow rate	1 mL/min (constant flow)
Carrier gas	He (99.999%)
Oven temperature	40 °C ® 5 °C/min ® 300 °C
Transfer line temperature	280
Mass spectrometer conditions	
Instrument	5977B (Agilent, Santa Clara, CA, USA)
Ion source temperature	230 °C
Ion source mode	EI mode
Electron energy	−70 eV
Scan type	Full-scan mode
Mass range (mu)	35–350
Other information	
Detection information	Micro- and nano-plastics

 doi:10.20944/preprints202603.0569.v1

Detection limit (μg)	PE (1.6), PP (0.44), PET (0.7), PA6 (0.5), PS (0.2), PMMA (0.2), and SBR (0.3)
Sample mass	~50 mg, Sample cup (~900 μℓ)

2.6. Fourier Transform Infrared Spectroscopy

Fourier transform infrared (FTIR) spectra were recorded using a LUMOS instrument equipped with an attenuated total reflectance (ATR) accessory. Each spectrum was collected in the range of 7000–650 cm^{-1} at a resolution of 2 cm^{-1} with 32 scans per sample. The main FTIR absorption wavelengths of PE and its corresponding functional groups were as follows: 2915–2920 cm^{-1} (-CH_2- asymmetric stretching), 2848–2850 cm^{-1} (-CH_2- symmetric stretching), 1465–1470 cm^{-1} (-CH_2- scissoring or bending), and 718 cm^{-1} (-CH_2- rocking). The detailed specifications of the instrument are listed in Table 4.

Table 4. FT-IR microscopy conditions.

FT-IR Microscope	
Instrument	LUMOS (Bruker Optics, Ettingen, Germany)
Detection type	Midband MCT
Objective	Schwarzschild objective 8×
Cooling type	Liquid nitrogen (N_2)
Spectral resolution	<2 cm^{-1}
Spectral range	7000–650 cm^{-1}
Measurement mode	Transmission, Reflection, μ-ATR

2.7. Raman Microscopy Analysis

Microscopic Raman spectra were recorded using an XploRa PLUS (HORIBA, Kyoto, Japan). The main Raman spectra of PE and its corresponding functional groups were as follows: 2881–2885 cm^{-1} (-CH_2- asymmetric stretching), 2848 cm^{-1} (-CH_2- symmetric stretching), and 1415–1440 cm^{-1} (-CH_2- bending). The detailed specifications of the instrument are listed in Table 5

Table 5. Raman microscopy conditions.

Raman Microscope	
Instrument	XploRa PLUS (HORIBA, Kyoto, Japan)
Detector	1024 × 256 BIDD TE air-cooled scientific CCD
Laser	532 nm
Power	Initial output: 100 mW (Filter: 100%, 50%, 25%, 10%, 1%, 0.1%)
Grating	600 grmm, 1200 grmm, 1800 grmm, 2400 grmm
Objective	x5 (N.A 0.1), x10 (N.A 0.25), x20 (N.A 0.45), x50 (N.A 0.8), x100 (N.A 0.9)

Microscope-Raman	
Instrument	XploRa PLUS(HORIBA, Japan)
Detector	1024 x 256 BIDD TE air cooled scientific CCD
Laser	532 nm
Power	Initial Output:100 mW (Filter: 100%, 50%, 25%, 10%, 1%, 0.1%)
Grating	600 grmm, 1200 grmm, 1800 grmm, 2400 grmm
Objective	x5 (N.A 0.1), x10 (N.A 0.25), x20 (N.A 0.45), x50 (N.A 0.8), x100 (N.A 0.9)

 doi:10.20944/preprints202603.0569.v1

3. Results

3.1. Decomposition Rate

The polymer-coated CRFs exhibited progressive degradation under simulated sunlight exposure. Weight loss measurements indicated approximately 50.0 ± 4.7% mass reduction after 10 days and 100.1 ± 2.1% after 60 days, whereas LN40 controls exhibited a degradation ratio that was three times lower (14.0 ± 1.9 - 31.0 ± 6.0%). These results confirm that LN40 with TiO2 significantly accelerated the photodegradation of the polymer coatings (Figures 1 and 2).

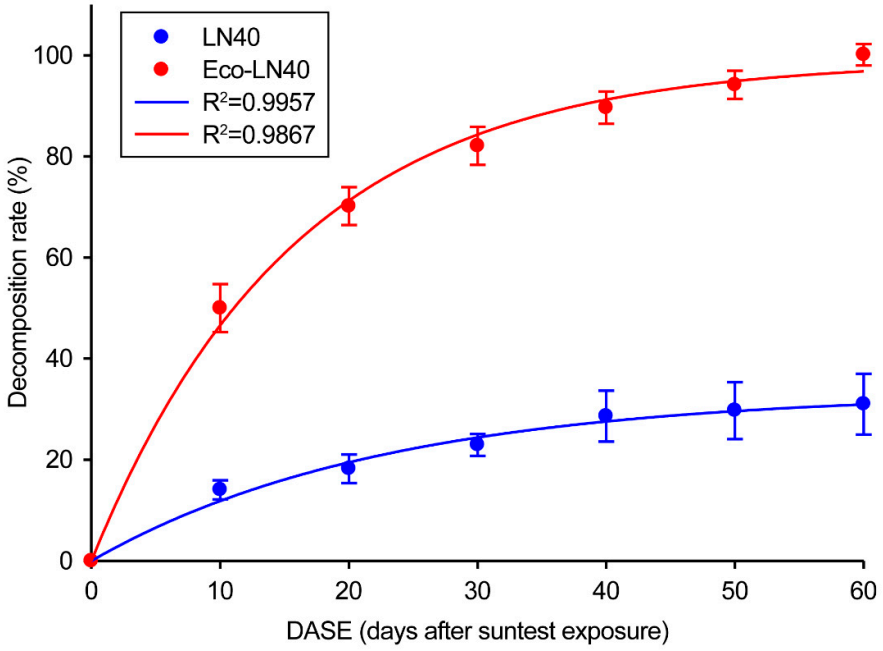

Figure 1. Decomposition rate of DASE.

 doi:10.20944/preprints202603.0569.v1

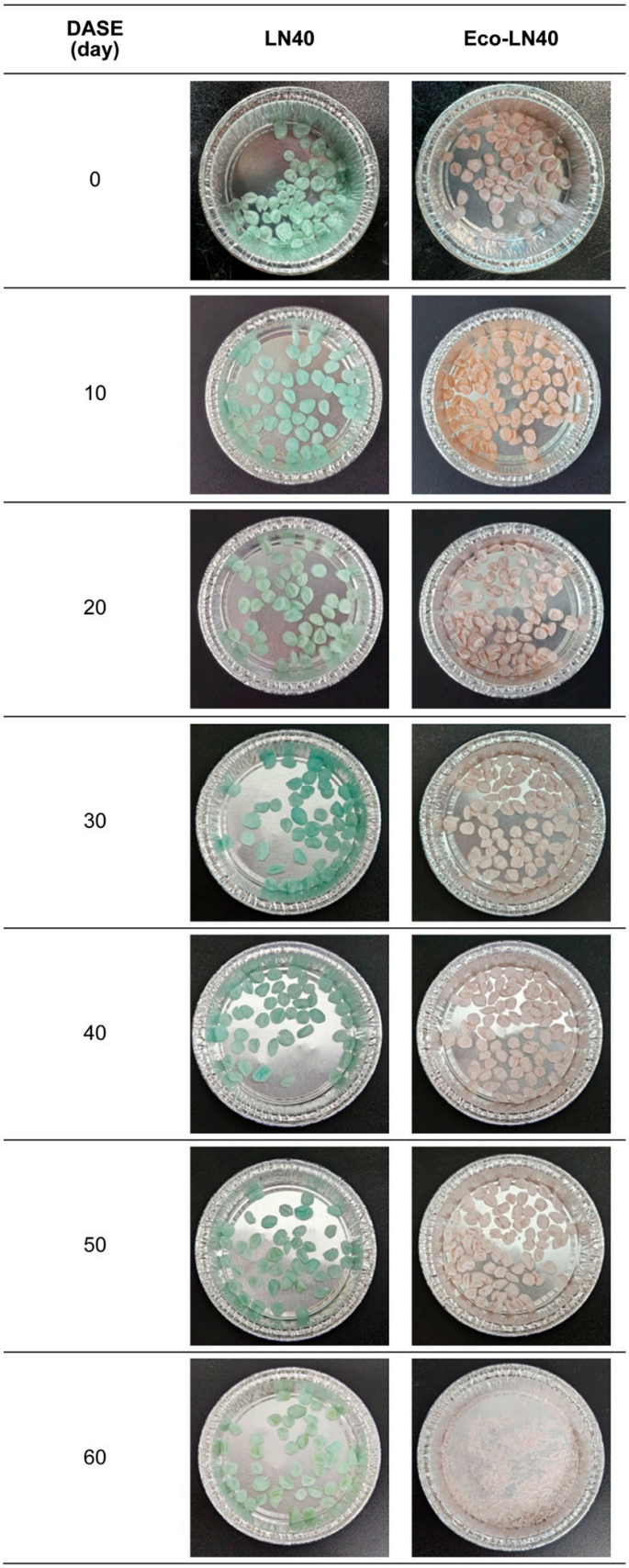

Figure 2. Decomposition LN40 and Eco-LN40.

 doi:10.20944/preprints202603.0569.v1

3.2. Surface Morphology Changes and Element Composition

SEM images revealed substantial surface alterations during photodegradation. Initially, the morphology of the CRF coatings was smooth and continuous, which is typical of intact polymeric films. Extensive fragmentation and peeling were observed in Eco-LN40 after 60 days of irradiation. However, after 60 d of irradiation, small cracks and voids appeared in LN40 (Figure 3). The analysis of the initial samples (LN40 and Eco-LN40 on day 0) revealed similar EDS results for C, O, Mg, and Si, excluding Ti. Therefore, Eco-LN40 was confirmed to have the same composition as LN40, and only the photodegradable components were added. In addition, trace amounts of Ca, presumably from contamination during the pretreatment and analysis processes, were detected in Eco-LN40 on day 60 of photodegradation (Table 6).

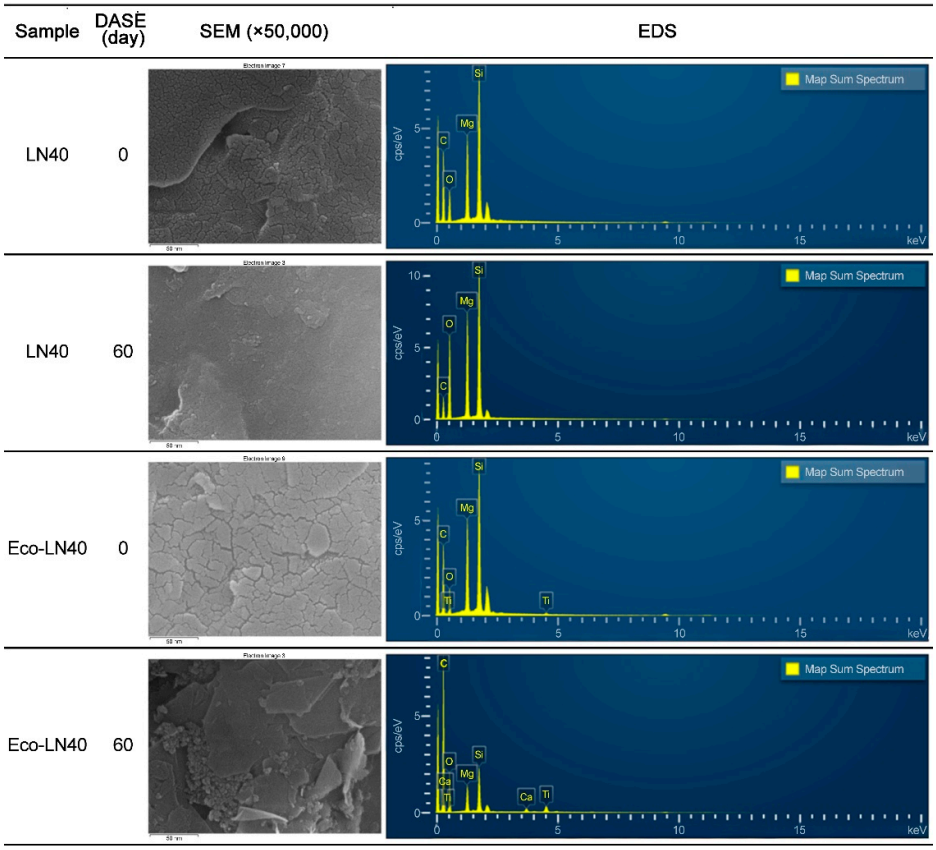

Figure 3. SEM-EDS graphs.

Table 6. EDS results.

Element	LN40 0 Day			LN40 60 Days			Eco-LN40 0 Day			Eco-LN40 60 Days		
	Wt%	Wt% Sigma	Atomic %	Wt%	Wt% Sigma	Atomic %	Wt%	Wt% Sigma	Atomic %	Wt%	Wt% Sigma	Atomic %
C	60.87	0.29	72.54	31.41	0.30	42.42	61.46	0.27	73.61	67.54	0.24	76.03
O	18.01	0.24	16.11	38.71	0.22	39.25	15.73	0.23	14.14	23.76	0.24	20.08
Mg	7.39	0.07	4.35	11.94	0.08	7.97	8.39	0.07	4.97	2.41	0.03	1.34
Si	13.73	0.11	7.00	17.95	0.10	10.37	13.95	0.10	7.15	3.74	0.04	1.80
Ca	-	-	-	-	-	-	-	-	-	0.62	0.03	0.21
Ti	-	-	-	-	-	-	0.47	0.04	0.14	1.93	0.05	0.54
Total	100	-	100	100	-	100	100	-	100	100	-	100

 doi:10.20944/preprints202603.0569.v1

3.3. Chemical Structure Evolution

TED-GC/MS, FTIR, and micro-Raman spectroscopy revealed significant chemical transformations in the coating materials. TED-GC/MS analysis revealed PE peaks in LN40 before and after 60 d of photolysis. PE peaks in Eco-LN40 were detected during the experiment, but no PE peaks were detected after photolysis for 60 d (Figure 4). The FTIR qualitative PE analysis showed that PE has absorption wavelengths of 2914, 2847, 1470, and 718 cm-^{1}. LN-40 and Eco-LN40 contained the same resin (PE) before photolysis. In LN40, PE peaks (2914, 2847, and 1470 cm^{-1}) were detected before and after 60 d of photolysis, but the 718 cm^{-1} peak was difficult to distinguish due to noise. However, in Eco-LN40, PE peaks were detected before the photolysis, but after 60 d of photolysis, the PE peaks at 2914, 2847, and 1470 cm^{-1} were not detected. The 718 cm^{-1} peak was difficult to distinguish due to noise (Figure 5). Raman analysis showed that PE exhibits absorption wavelengths around 2847.66 cm^{-1} and 2880.52 cm^{-1}. In LN40, PE peaks at 2847.47 and 2881.48 cm^{-1} were detected after 60 days of photodegradation. However, in Eco-LN40, PE peaks at 2847.66 and 2880.52 cm^{-1} were not detected after 60 days of photodegradation (Figure 6). These results demonstrate that the polymer matrix of ECO-LN40, which contains photocatalysts undergoes oxidation and chain scission during photolysis.

 doi:10.20944/preprints202603.0569.v1

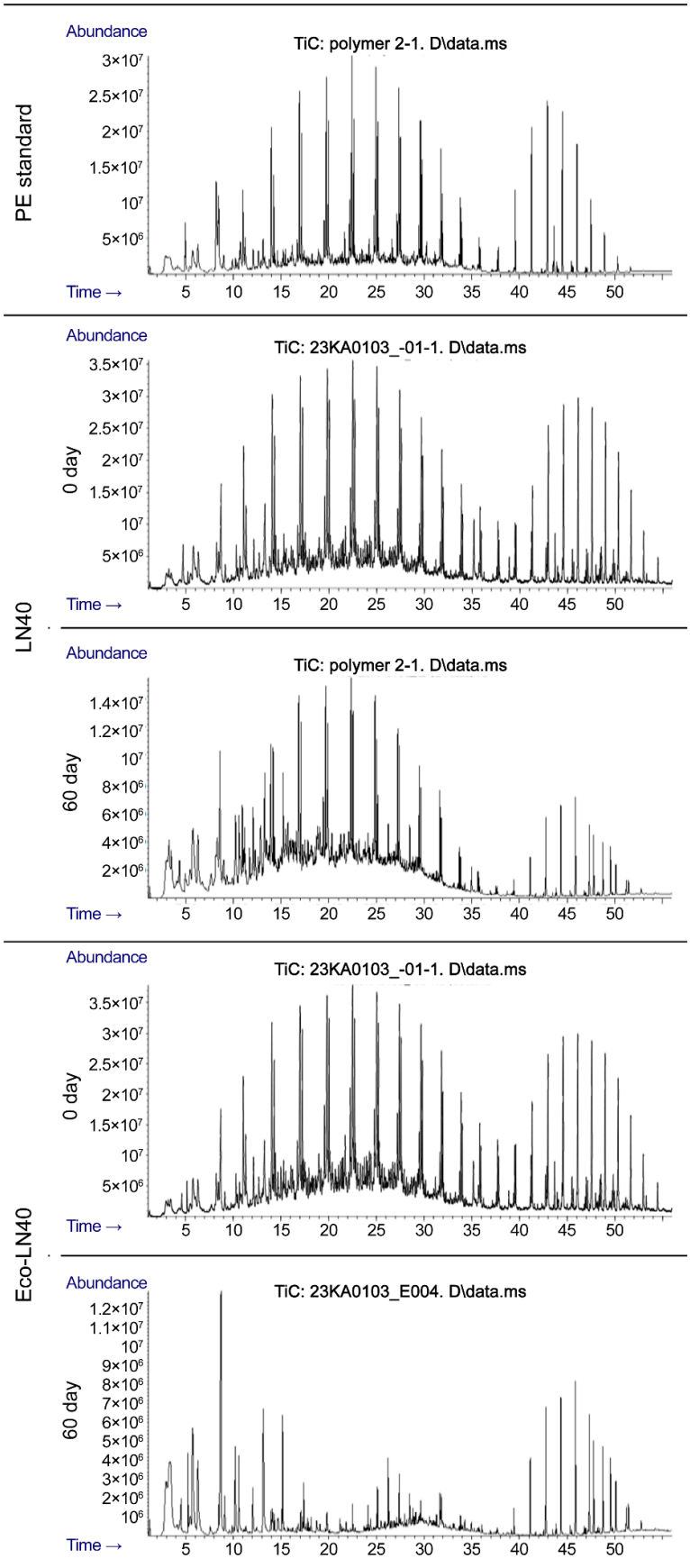

Figure 4. TED-GC/MS chromatograms.

 doi:10.20944/preprints202603.0569.v1

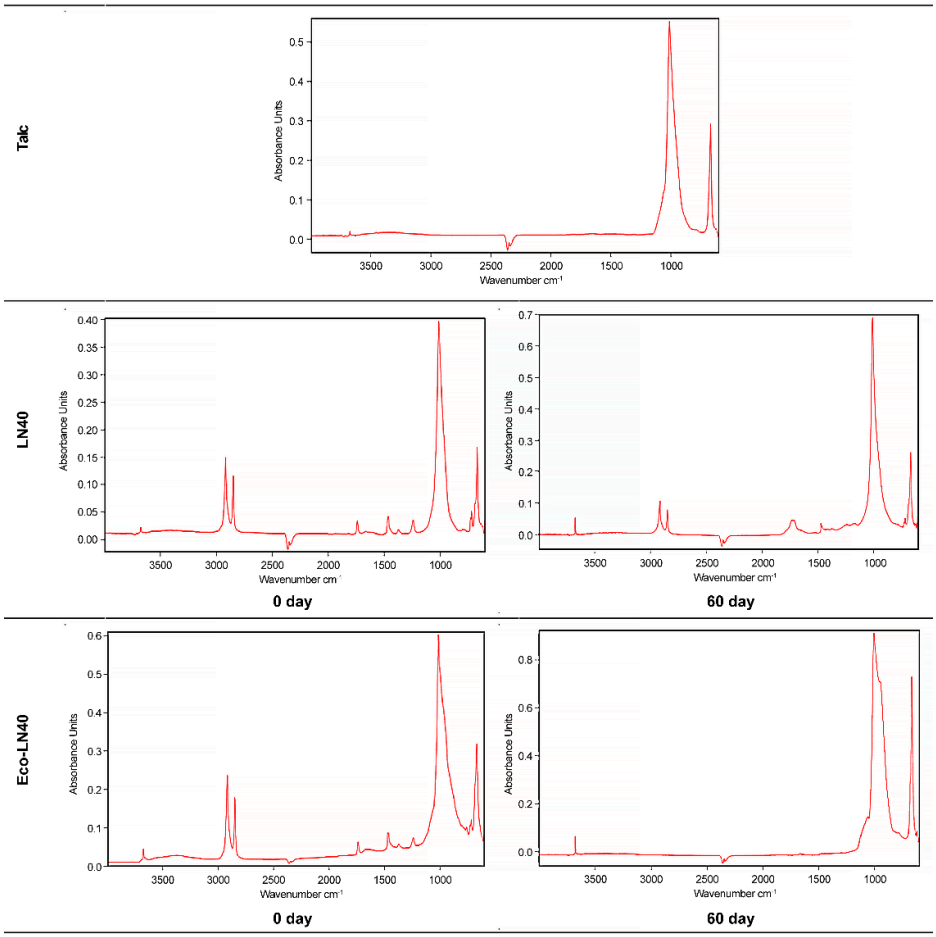

Figure 5. FT-IR Chromatograms.

 doi:10.20944/preprints202603.0569.v1

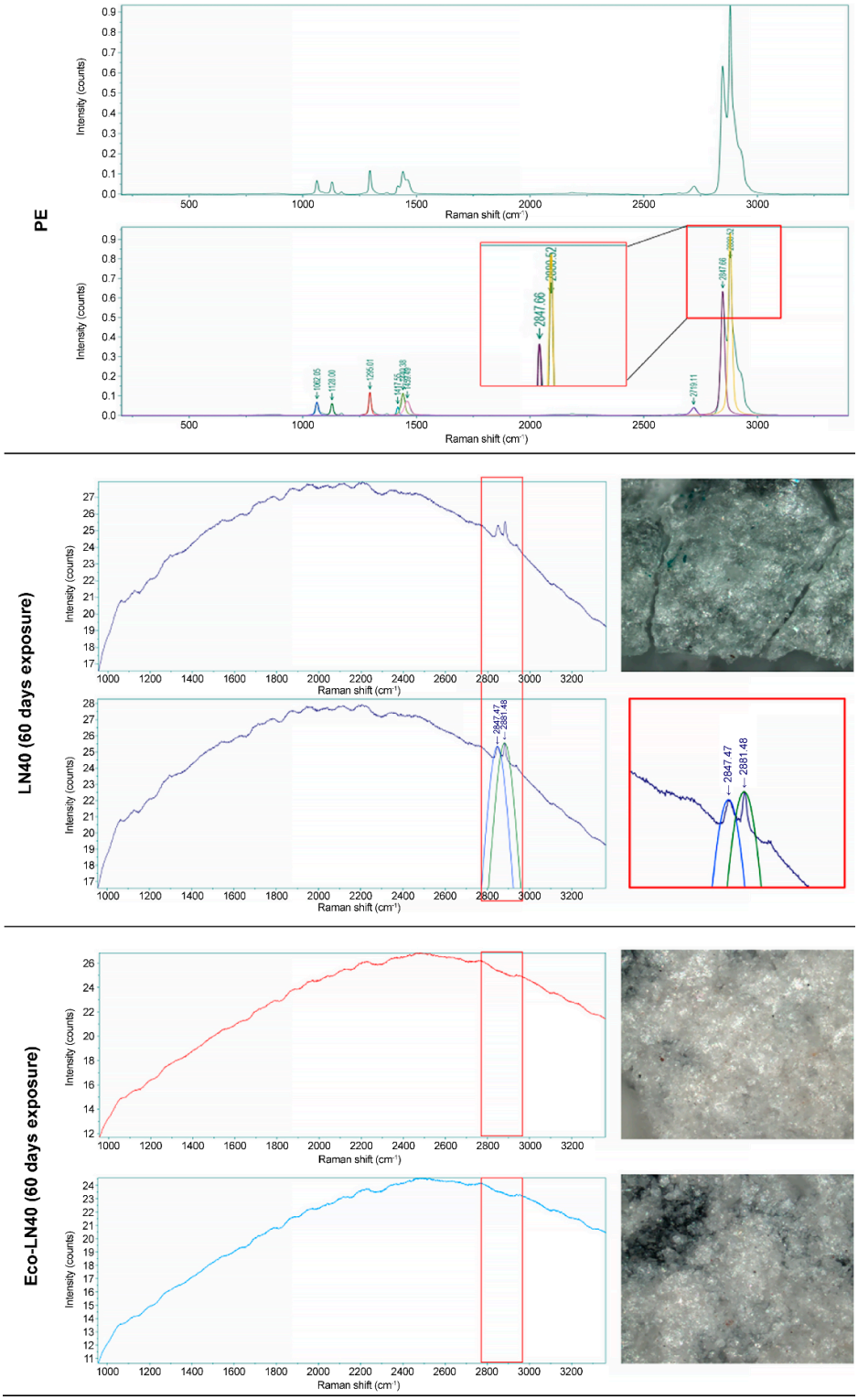

Figure 6. Raman chromatograms.

4. Discussion

The results of this study demonstrate that the incorporation of TiO_2 photocatalysts into polymer-coated controlled-release fertilizers (CRFs) substantially enhances the degradation of polyethylene-based coating materials under simulated solar irradiation. Eco-LN40 exhibited complete degradation

 doi:10.20944/preprints202603.0569.v1

after 60 days of irradiation, whereas the conventional CRF (LN40) showed only limited degradation (14–31%). These findings indicate that photocatalytic oxidation can significantly accelerate the breakdown of otherwise persistent polyolefin coatings.

Polyethylene-based polymers are widely used in fertilizer coatings because of their durability and low permeability; however, these properties also result in long environmental persistence. Polyethylene materials are known to resist biodegradation and may persist in soils for decades or even centuries, undergoing slow photooxidative weathering that mainly results in fragmentation rather than complete mineralization [13]. During environmental weathering, polymer chains experience oxidative chain scission, embrittlement, and fragmentation, ultimately generating micro- and nanoplastic particles [7]. These secondary plastic fragments can accumulate in soils and aquatic systems and have become an emerging global environmental concern [8].

Recent studies have identified polymer coatings used in agricultural fertilizers as an overlooked source of microplastics in soils. Because CRFs are applied repeatedly during crop production cycles, coating residues may accumulate in agricultural soils and contribute to the long-term buildup of plastic debris [11]. Cusworth et al. (2024) estimated that fertilizer applications can contribute substantially to microplastic concentrations in agricultural soils, highlighting the importance of evaluating the environmental fate of fertilizer coating materials [24]. Microplastics present in soils have been shown to influence soil aggregation, microbial activity, and plant root development, potentially altering nutrient cycling and soil ecosystem functioning [10,25]. Moreover, microplastic particles can adsorb organic contaminants and heavy metals, thereby facilitating the transport of pollutants through soil–water systems [14].

The accelerated degradation observed in Eco-LN40 can be explained by the photocatalytic activity of TiO_2 incorporated within the coating matrix. When exposed to ultraviolet or visible light, TiO_2 generates electron–hole pairs that react with oxygen and water molecules to form reactive oxygen species (ROS), including hydroxyl radicals (•OH) and superoxide radicals (O_2•$^-$) [16–18]. These highly reactive species initiate oxidative degradation by abstracting hydrogen atoms from polyethylene chains and cleaving C–C bonds within the polymer backbone. The resulting oxidative reactions progressively shorten polymer chains and form oxygen-containing functional groups such as carbonyl and carboxyl groups, which may subsequently undergo further oxidation and mineralization into CO_2 and H_2O [9,16]. Similar photocatalytic degradation pathways have been widely reported for polyethylene materials containing pro-oxidant additives or TiO_2-based photocatalysts [17,18,26].

Morphological evidence obtained from SEM observations supports the occurrence of extensive oxidative degradation in Eco-LN40. The initially smooth and continuous polymer coating developed severe fragmentation and peeling after prolonged irradiation, whereas LN40 showed only minor cracks and surface defects. These structural changes are characteristic of polyethylene photooxidation, where oxidative chain scission reduces the mechanical integrity of polymer films and ultimately leads to fragmentation [7]. The EDS analysis revealed enrichment of Ti in Eco-LN40 coatings, confirming the presence of the photocatalyst and suggesting that TiO_2 remained associated with the degrading polymer matrix throughout the irradiation period.

Chemical characterization using TED-GC/MS, FTIR, and Raman spectroscopy provided further evidence for the degradation pathway of the coating materials. Polyethylene signals were detected in LN40 both before and after photodegradation, indicating that the polymer structure remained largely intact despite irradiation. In contrast, polyethylene signals were not detected in Eco-LN40 after 60 days of irradiation. Consistent trends were observed in FTIR and Raman spectra, where characteristic polyethylene absorption bands (2914, 2847, and 1470 cm^{-1}) remained detectable in LN40 but disappeared in Eco-LN40. The disappearance of these spectral features suggests that the polyethylene backbone underwent extensive oxidation and degradation rather than simple fragmentation into smaller plastic particles.

Importantly, the absence of detectable polyethylene residues in Eco-LN40 suggests that photocatalytic degradation may suppress the formation of secondary microplastic particles during

 doi:10.20944/preprints202603.0569.v1

CRF weathering. Conventional polyethylene coatings typically degrade through incomplete oxidation pathways that produce microplastic fragments as intermediate products [7]. In contrast, photocatalytic systems may promote deeper oxidative degradation of polymer chains, potentially preventing the accumulation of persistent microplastic residues.

From a novelty perspective, this study provides direct analytical evidence that TiO_2-mediated photocatalytic degradation of CRF coatings can proceed without detectable polyethylene microplastic residues. While previous studies have suggested that fertilizer coatings may contribute to microplastic accumulation in soils, experimental confirmation of degradation pathways and residue formation during CRF weathering has remained limited. The combined use of TED-GC/MS, FTIR, Raman spectroscopy, and SEM-EDS in this study provides complementary evidence supporting the complete disappearance of polyethylene signals in photocatalytic CRF coatings.

This finding has important environmental implications for agricultural systems. Controlled-release fertilizers are increasingly used worldwide to improve nutrient use efficiency and reduce nutrient losses from soils [1–4]. However, concerns have been raised regarding the persistence of synthetic polymer coatings in soils and their potential contribution to plastic pollution in agroecosystems [5,11]. The development of photocatalytic fertilizer coatings capable of undergoing rapid degradation under sunlight exposure may therefore represent a promising strategy for reducing the environmental footprint of CRF technologies and mitigating the risk of microplastic contamination in agricultural soils.

Despite these promising findings, several limitations should be considered. First, the photodegradation experiments were conducted under controlled laboratory conditions using xenon-arc irradiation designed to simulate sunlight exposure. In real agricultural environments, degradation behavior may be influenced by additional factors such as soil burial, shading by crop canopies, seasonal temperature fluctuations, moisture dynamics, and microbial activity. These environmental factors may significantly alter degradation kinetics compared with laboratory simulations. Second, although spectroscopic analyses confirmed the disappearance of detectable polyethylene signals, further studies employing complementary quantitative techniques such as pyrolysis-GC/MS or isotopic carbon tracing would help determine the extent of polymer mineralization and identify potential intermediate degradation products.

Future research should therefore focus on long-term field evaluations of photocatalytic CRF coatings under realistic agricultural conditions. Such studies should assess degradation behavior in soils, monitor potential intermediate products, and evaluate ecological impacts on soil organisms and crop systems. These investigations will be essential for developing next-generation fertilizer coatings that combine agronomic efficiency with environmental sustainability.

This study provides mechanistic evidence that photocatalytic CRF coatings may represent a viable strategy for mitigating microplastic pollution originating from agricultural fertilizer inputs

5. Conclusions

Evidence of microplastic formation from CRFs raises serious concerns regarding their long-term environmental safety. Agricultural soils may accumulate these particles through repeated fertilizer applications, potentially affecting soil porosity, microbial activity, and plant-root interactions [10]. Runoff and erosion can transport these microplastics into aquatic ecosystems where they may persist for extended periods. These findings underscore the need to reconsider polymer selection in CRF formulations and develop biodegradable or photodegradable alternatives that minimize plastic pollution in agroecosystems. Accordingly, this study aimed to minimize these environmental impacts by comparing the decomposition rate and residual microplastic content of Eco-CRF, a coating material containing a catalyst that promotes photodegradation, with those of the conventional CRF LN40**.** The results confirmed that the coating shell of general CRFs, which are composed of synthetic resin, requires an extremely long time (over 100 years) to decompose under natural conditions, placing a potential burden on soil and aquatic environments. Furthermore, even when the CRF`s resin coating degrades, it can be converted into microplastics, thereby raising environmental

 doi:10.20944/preprints202603.0569.v1

concerns similar to those of conventional CRFs. However, in this study, TED-GC/MS, FT-IR, and Raman analyses of Eco-CRF showed 100% decomposition (based on weight loss), as no PE was detected. This indicates that the material was completely decomposed and not converted into microplastics. The results of this study can to serve as fundamental data for carbon neutrality initiatives and provide an early response framework for potential environmental issues in the agricultural sector while addressing concerns regarding microplastic contamination.

Author Contributions: H.-W.J.: Conceptualization, Data curation, Formal analysis, Visualization, Writing-original draft, Writing- review and editing. J.-S.L.: Methodology, Data curation, and Formal analysis. I.J.: Methodology, Data curation, Formal analysis. Y.-I.C.: Methodology, Data curation, Formal analysis. J.-K.M.: Conceptualization, Funding acquisition, project administration, Supervision, Writing-review, and editing. All authors have read and agreed to the published version of the manuscript.

Funding: This study was supported and grant funded by Farmhannong Co., Ltd.

Institutional Review Board Statement: Not applicable

Informed Consent Statement: Not applicable.

Data Availability Statement: The original contributions presented in this study are included in the article. Further inquiries can be directed to the corresponding authors.

Conflicts of Interest: The authors declare no conflicts of interest.

Abbreviations

The following abbreviations are used in this manuscript:

CRF	Controlled-Release Fertilizer
SEM-EDS	Scanning Electron Microscopy-Energy Dispersive Spectroscopy
TED-GC/MS	Thermal Extraction Desorption Gas Chromatograph Mass Spectrometer
FTIR	Fourier Transform Infrared
DASE	Day After Suntest Exposure

References

1. Shaviv, A. Advances in controlled-release fertilizers. *Adv. Agron.* **2001**, *71*, 1–49. https://doi.org/10.1016/S0065-2113(01)71011-5.
2. Trenkel. Slow- and Controlled-Release and Stabilized Fertilizers: An Option for Enhancing Nutrient Use Efficiency in Agriculture, 2nd ed.; IFA Publication: Paris, France, 2010.
3. Li, X.; Li, Z. Global trends and current advances in slow/controlled-release fertilizers: A bibliometric analysis from 1990 to 2023. *Agriculture* **2024**, *14*, 1502. https://doi.org/10.3390/agriculture14091502.
4. Lawrencia, D.; Wong, S.K.; Low, D.Y.S.; Goh, B.H.; Goh, J.K.; Ruktanonchai, U.R.; Soottitantawat, A.; Lee, L.H.; Tang, S.Y. Controlled release fertilizers: A review on coating materials and mechanism of release. *Plants* **2021**, *10*, 238. https://doi.org/10.3390/plants10020238.
5. Yang, L.; An, D.; Wang, T.-J.; Kan, C.; Jin, Y. Photodegradation of Polymer Materials Used for Film Coatings of Controlled-Release Fertilizers. *Chem. Eng. Technol.* **2017**, *40*, 1611–1618. https://doi.org/10.1002/ceat.201600120.
6. Li, J.; Wang, D.; Chen, T.; Zhou, W.; Zhan, X. Risks of microplastics from polyurethane and polyethylene-polycarbonate coated fertilizers to soil-crop system. *J. Hazard. Mater.* **2025**, *499*, 140181. https://doi.org/10.1016/j.jhazmat.2025.140181.
7. Song, Y.K.; Hong, S.H.; Eo, S.; Shim, W.J. The fragmentation of nano-and microplastic particles from thermoplastics accelerated by simulated-sunlight-mediated photooxidation. *Environ. Pollut.* **2022**, *311*, 119847. https://doi.org/10.1016/j.envpol.2022.119847.
8. Thompson, R.C.; Olsen, Y.; Mitchell, R.P.; Davis, A.; Rowland, S.J.; John, A.W.; Mcgonigle, D.; Russell, A.E. Lost at sea: Where is all the plastic? *Science* **2004**, *304*, 838. https://doi.org/10.1126/science.1094559.

 doi:10.20944/preprints202603.0569.v1

9. Xu, J.; Yang, W.; Zhang, C.; Dong, X.; Luo, Y. Photo-oxidation and biodegradation of polyethylene films containing polyethylene glycol modified TiO_2 as pro-oxidant additives. *Polym. Compos.* **2018**, *39*, E531–E539. https://doi.org/10.1002/pc.24679.
10. Rillig, M.C.; Lehmann, A.; de Souza Machado, A.A.; Yang, G. Microplastic effects on plants. *New Phytol.* **2019**, *223*, 1066–1070. https://doi.org/10.1111/nph.15794.
11. Cusworth, S.J.; Davies, W.J.; McAinsh, M.R.; Gregory, A.S.; Storkey, J.; Stevens, C.J. Agricultural fertilisers contribute substantially to microplastic concentrations in UK soils. *Commun. Earth Environ.* **2024**, *5*, 7. https://doi.org/10.1038/s43247-023-01172-y.
12. Shao, Z.; Xiao, K.Q.; Jin, M.; Chen, S.; Huo, Y.; Zhu, Y.G. Environmental fate and effects of mulch films on agricultural soil: A systematic review from application to residual impact. *Crit. Rev. Environ. Sci. Technol.* **2025**, *56*, 43–66. https://doi.org/10.1080/10643389.2025.2580771.
13. Gewert, B.; Plassmann, M.M.; MacLeod, M. Pathways for degradation of plastic polymers floating in the marine environment. *Environ. Sci. Process. Impacts* **2015**, *17*, 1513–1521. https://doi.org/10.1039/C5EM00207A.
14. Mai, L.; Bao, L.J.; Wong, C.S.; Zeng, E.Y. Microplastics in the terrestrial environment. In *Microplastic Contamination in Aquatic Environments*; Elsevier: Amsterdam, The Netherlands, 2024; pp. 229–247. https://doi.org/10.1016/B978-0-443-15332-7.00012-0.
15. Lee, Q.Y.; Li, H. Photocatalytic degradation of plastic waste: A mini review. *Micromachines* **2021**, *12*, 907. https://doi.org/10.3390/mi12080907.
16. Ge, J.; Zhang, Z.; Ouyang, Z.; Shang, M.; Liu, P.; Li, H.; Guo, X. Photocatalytic degradation of (micro)plastics using TiO_2-based and other catalysts: Properties, influencing factor, and mechanism. *Environ. Res.* **2022**, *209*, 112729. https://doi.org/10.1016/j.envres.2022.112729.
17. Singh, S.; Mahalingam, H.; Singh, P.K. Polymer-supported titanium dioxide photocatalysts for environmental remediation: A review. *Appl. Catal. A* **2013**, *462–463*, 178–195. https://doi.org/10.1016/j.apcata.2013.04.039.
18. Coromelci, C.G.; Turcu, E.; Doroftei, F.; Palamaru, M.N.; Ignat, M. Conjugated polymer modifying TiO2 performance for visible-light photodegradation of organics. *Polymers* **2023**, *15*, 2805. https://doi.org/10.3390/polym15132805.
19. ASTM G151-19; Standard practice for exposing nonmetallic materials in accelerated test devices that use laboratory light sources. ASTM International: West Conshohocken, PA, USA, **2019**. https://doi.org/10.1520/G0151-19
20. ASTM G155-21; Standard practice for operating xenon arc lamp apparatus for exposure of materials, ASTM International: West Conshohocken, PA, USA, **2021**. https://doi.org/10.1520/G0155-21
21. ASTM D5071-06; Standard practice for exposure of photodegradable plastics in a xenon arc apparatus, ASTM International: West Conshohocken, PA, USA, **2022**. https://doi.org/10.1520/D5071-06R21
22. KS M 4892-1; Plastics-Methods of exposure to laboratory light sources-Part 1 : General guidance, Korean Agency for Technology and Standards: Eumseong, Chungcheongbuk-do, Republic of Korea, **2022**.
23. *ISO/TC 147/SC 2/JWG 1*; Joint ISO/TC 147/SC 2—ISO/TC 661/SC 14 WG: Plastics (Including Microplastics) in Waters and Related Matrices. ISO: Geneva, Switzerland, **2024**.
24. Cusworth, S. J.; Davies, W. J.; McAinsh, M. R.; Gregory, A. S.; Storkey, J.; Stevens, C. J. Agricultural fertilisers contribute substantially to microplastic concentrations in UK soils. *Communications Earth & Environment* **2024**, 5(1), 7. https://doi.org/10.1038/s43247-023-01172-y
25. de Souza Machado, A. A.; Kloas, W.; Zarfl, C.; Hempel, S.; & Rillig, M. C. Microplastics as an emerging threat to terrestrial ecosystems. *Global change biology*. **2018**, 24(4), 1405-1416. https://doi.org/10.1111/gcb.14020
26. Ge, J.; Zhang, Z.; Ouyang, Z.; Shang, M.; Liu, P.; Li, H.; Guo, X. Photocatalytic degradation of (micro)plastics using TiO_2-based catalysts: Mechanisms and environmental applications. *Environmental Research* **2022**, 209, 112729. https://doi.org/10.1016/j.envres.2022.112729